

- latitude (6) and increase with increasing altitude (29).  $\delta D$  values in precipitation and surface waters [and ultimately in plant and animal tissues (14)] vary as a function of latitude, altitude, season, and distance inland (30, 31).  $\delta D$  values tend to decrease with increasing latitude in a northwesterly direction across North America (6–8, 14) and decrease with increasing altitude (30, 31).
16. Isotopic ratios ( $R$ ) of carbon and hydrogen are reported in  $\delta$  units:  $\delta = [(R_{\text{sample}}/R_{\text{standard}}) - 1] \times 1000$ .  $\delta^{13}\text{C} \pm 0.22$  per mil (‰), reported as the ratio of  $^{13}\text{C}/^{12}\text{C}$ ‰ relative to the Pee Dee belemnite standard, was analyzed with online analytical techniques (9). Mesquite plant standards of known isotopic composition (9) were used to systematically correct all of the online feather values to previously published offline values (6).  $\delta D \pm 5$ ‰, reported as the ratio of  $^2\text{H}/^1\text{H}$ ‰ relative to the Vienna standard mean ocean water standard, of wintering ground samples was analyzed with online analytical techniques (32). All of the feathers analyzed online for  $\delta D$  had remained at one location (Dartmouth College, NH) for at least 4 years and were analyzed over a 5-day period to minimize possible exchange with ambient water vapor. Breeding ground  $\delta D$  values were taken from previously reported values run with offline analytical techniques [exchangeable hydrogen was standardized before analysis by means of a high-temperature preparative equilibrium technique (6)]. We analyzed 15 feathers both offline and online.  $\delta D$  values did not significantly differ between the techniques ( $t_{15} = 0.77$ ,  $P = 0.46$ ), so no systematic correction was needed to compare the data sets.
17. The black-throated blue warbler is suitable as a study species because its breeding range covers a wide north-south gradient of  $\sim 17^\circ$  latitude, as well as a wide east-west gradient of  $\sim 26^\circ$  longitude across the northern portion of the breeding range (Fig. 1). It is mainly restricted to continuous tracts of undisturbed deciduous or mixed deciduous/coniferous forest habitat on mountainous slopes or at high elevation, where it feeds primarily on arthropods gleaned from foliage (12). Because the black-throated blue warbler is restricted almost exclusively to forested habitat,  $\delta^{13}\text{C}$  in its feathers is not complicated by  $\text{C}_4$  crops in agricultural fields (8).
18. Breeding ground samples consisted of flank feathers (nine sites) and tail feathers (one site), usually the third rectrix, from juvenile ( $<1$  year) and adult ( $>1$  year) male birds. There was no significant difference in  $\delta^{13}\text{C}$  between flank and tail feathers from within birds ( $t_{27} = 1.36$ ,  $P = 0.19$ ). Feather samples from NC were not analyzed for  $\delta D$ , and different samples from NH were analyzed for  $\delta^{13}\text{C}$  and  $\delta D$ , so samples from these sites could not be used in the regression models (20, 21). Samples from 8 of 10 breeding sites were collected within a single year (during 1989–1998), whereas birds from WV were sampled over 2 years and those from NH over 6 years. Although only male feather samples were used in all of the breeding ground analyses, we also examined a group of females from NH. With one exception, there were no significant effects of age, sex (NH only), or year, or their interactions, on  $\delta^{13}\text{C}$  (WV:  $F_{1,29} < 3.72$ ,  $P > 0.05$ ; NH:  $F < 1.76$ ,  $P > 0.05$ ,  $df = 1$  to 5 and 58); a significant effect of year for  $\delta^{13}\text{C}$  in NH ( $F_{5,59} = 4.64$ ,  $P = 0.002$ ) was due to high values in 1 of 6 years (mean  $\pm$  SE =  $-23.2 \pm 0.34$  in 1994 versus means of  $-24.4$  to  $-24.9$  for all other years). Wintering ground samples consisted of single tail feathers, usually the third rectrix, from juveniles ( $<10$  year) and adults ( $>1$  year) of both sexes. Samples from two of the Jamaica sites were not analyzed for  $\delta D$ . Each of the wintering sites was sampled in multiple years (1989–1997), and years did not differ in isotope ratios ( $\delta^{13}\text{C}$ :  $F_{20,349} = 1.55$ ,  $P > 0.05$ ;  $\delta D$ :  $F_{12,123} = 0.58$ ,  $P > 0.05$ ; year nested within site).
19. Breeding sites sampled in the southern portion of the breeding range tended to be at higher elevation than those in the north ( $F_{1,8} = 23.74$ ,  $P = 0.0012$ ,  $r^2 = 0.75$ ). Although  $\delta^{13}\text{C}$  tends to increase (28, 29) and  $\delta D$  tends to decrease (30, 31) with increasing altitude, the patterns we observed in feathers were due mainly to differences in the latitude of the sampling sites and not in the altitude at which the birds were captured ( $\delta^{13}\text{C}$ : latitude,  $F_{1,266} = 14.62$ ,  $P = 0.0002$ ; altitude,  $F_{1,266} = 2.57$ ,  $P = 0.11$ ; interaction,  $F_{1,266} = 2.33$ ,  $P = 0.13$ .  $\delta D$ :

- latitude,  $F_{1,129} = 7.33$ ,  $P = 0.0077$ ; altitude,  $F_{1,129} = 2.62$ ,  $P = 0.11$ ; interaction,  $F_{1,129} = 2.38$ ,  $P = 0.13$ ). Furthermore, we sampled birds from over 500 m of elevation at the NC site and found no effect of altitude on  $\delta^{13}\text{C}$  ( $F_{1,28} = 0.57$ ,  $P = 0.46$ ,  $r^2 = 0.02$ ).
20. We fit a regression model using both isotopes as independent variables. Breeding latitude =  $-12.55 - 1.95(\delta^{13}\text{C}) - 0.097(\delta D)$  ( $R^2 = 0.44$ ,  $n = 129$ ,  $P < 0.0001$  for both  $\delta^{13}\text{C}$  and  $\delta D$ ). The model correctly predicted breeding latitude to  $\pm 3.18^\circ$  (MSE $^{0.5}$ ).
21. We fit a regression model matching that in (20) but predicting breeding longitude instead of latitude. Breeding longitude =  $115.51 + 2.62(\delta^{13}\text{C}) - 0.28(\delta D)$  ( $R^2 = 0.34$ ,  $n = 69$ ,  $P = 0.017$  and  $P < 0.0001$  for  $\delta^{13}\text{C}$  and  $\delta D$ , respectively). The model correctly predicted breeding longitude to  $\pm 6.40^\circ$  (MSE $^{0.5}$ ).
22. R. Greenberg, in *Migrant Birds in the Neotropics*, A. Keast, E. S. Morton, Eds. (Smithsonian Institution Press, Washington, DC, 1980), pp. 593–604.
23. B. B. DeWolfe, L. F. Baptista, *Condor* **97**, 376 (1995).
24. M. A. Ramos, D. W. Warner, in *Migrant Birds in the Neotropics*, A. Keast, E. S. Morton, Eds. (Smithsonian Institution Press, Washington, DC, 1980), pp. 173–180.
25. R. Pellek, *J. Forest.* **88**, 15 (1990).
26. K. Lajtha, J. D. Marshall, in *Stable Isotopes in Ecolog-*

- ical and Environmental Sciences*, K. Lajtha, R. H. Michener, Eds. (Oxford Univ. Press, London, 1994), pp. 1–21.
27. B. N. Smith, S. Epstein, *Plant Physiol.* **47**, 380 (1971).
28. C. Korner, G. D. Farquhar, S. C. Wong, *Oecologia* **88**, 30 (1991).
29. K. R. Hultine, J. D. Marshall, *Oecologia* **123**, 32 (2000).
30. W. Dansgaard, *Tellus* **16**, 436 (1964).
31. H. Ziegler, in *Stable Isotopes in Ecological Research*, P. W. Rundel, J. R. Ehleringer, K. A. Nagy, Eds. (Springer-Verlag, New York, 1988), pp. 105–123.
32. Z. D. Sharp, V. Atudorei, T. Durakiewicz, *Chem. Geol.* **178**, 197 (2000).
33. Supported by undergraduate research grants from Dartmouth College, the Howard Hughes Medical Institute, and the Andrew W. Mellon Foundation to D.R.R., as well as research grants from NSF to R.T.H. and C.P.C. and from the Smithsonian Institution to G.R.G. S. Latta, G. Wallace, and J. Wunderle provided feather samples from Hispaniola, Cuba, and Puerto Rico, respectively. X. Feng and M. Poage helped with the isotopic analyses. We thank S. Emlen, P. Marra, D. I. Rubenstein, P. Sherman, S. Sillett, and M. Wikelski for constructive comments.

15 October 2001; accepted 7 December 2001

## Melanopsin-Containing Retinal Ganglion Cells: Architecture, Projections, and Intrinsic Photosensitivity

S. Hattar,<sup>1,2\*</sup> H.-W. Liao,<sup>2\*</sup> M. Takao,<sup>4</sup> D. M. Berson,<sup>4</sup> K.-W. Yau<sup>1,2,3†</sup>

The primary circadian pacemaker, in the suprachiasmatic nucleus (SCN) of the mammalian brain, is photoentrained by light signals from the eyes through the retinohypothalamic tract. Retinal rod and cone cells are not required for photoentrainment. Recent evidence suggests that the entraining photoreceptors are retinal ganglion cells (RGCs) that project to the SCN. The visual pigment for this photoreceptor may be melanopsin, an opsin-like protein whose coding messenger RNA is found in a subset of mammalian RGCs. By cloning rat melanopsin and generating specific antibodies, we show that melanopsin is present in cell bodies, dendrites, and proximal axonal segments of a subset of rat RGCs. In mice heterozygous for tau-lacZ targeted to the melanopsin gene locus,  $\beta$ -galactosidase-positive RGC axons projected to the SCN and other brain nuclei involved in circadian photoentrainment or the pupillary light reflex. Rat RGCs that exhibited intrinsic photosensitivity invariably expressed melanopsin. Hence, melanopsin is most likely the visual pigment of phototransducing RGCs that set the circadian clock and initiate other non-image-forming visual functions.

Retinal rods and cones, with their light-sensitive, opsin-based pigments, are the primary photoreceptors for vertebrate vision. Visual sig-

nals are transmitted to the brain through RGCs, the output neurons whose axons form the optic nerve. This system, through its projections to the lateral geniculate nucleus and the midbrain, is responsible for interpreting and tracking visual objects and patterns. A separate visual circuit, running in parallel with this image-forming visual system, encodes the general level of environmental illumination and drives certain photic responses, including synchronization of the biological clock with the light-dark cycle (1), control of pupil size (2), acute sup-

<sup>1</sup>Howard Hughes Medical Institute and Departments of <sup>2</sup>Neuroscience and <sup>3</sup>Ophthalmology, Johns Hopkins University School of Medicine, 725 North Wolfe Street, Baltimore, MD 21205–2185, USA. <sup>4</sup>Department of Neuroscience, Brown University, Providence, RI 02912, USA.

\*These authors contributed equally to this work.  
†To whom correspondence should be addressed. E-mail: kwyau@mail.jhmi.edu

REPORTS

**Fig. 1.** Immunocytochemistry of melanopsin-containing RGCs in the flat-mounted rat retina. **(A)** Confocal images at the level of the ganglion cell layer showing labeling with the melanopsin NH<sub>2</sub>-terminal specific antibody. The fluorescent immunolabeling is in green, and the nuclei are stained by red fluorescent propidium iodide. Arrows 1 and 2 indicate axons associated with the indicated RGC cell bodies heading toward the optic disc. Note the beaded appearance of the dendrites. Because the image is at a particular focal plane, some dendrites and axons are not visible. **(B)** Nonstacked (1) and stacked (2) confocal images of the same retinal field from another preparation, but without nuclear counterstaining. The stacked picture combined all focal planes containing labeled processes. Note the peripheral localization of the melanopsin-labeling in the cell bodies in (B1). Because the stacking increased background, the sensitivity of the camera was reduced, making some faint processes not clearly visible. **(C)** Camera-lucida drawings of several melanopsin-positive RGCs, obtained from stacked images. The beaded appearance of the dendrites is not shown. The left and right panels show nondisplaced and displaced RGCs, respectively. The displaced cells have smaller and apparently more sparse dendritic fields. Arrows indicate axons. **(D)** Soma-size distribution of (a sample of) nondisplaced melanopsin-positive RGCs, which account for >95% of all labeled RGCs. **(E)** Overall distribution of melanopsin-positive RGCs on the flat-mounted right and left retinas of the same rat. Dozens of local dark-field images were taken separately at low magnification, and the montage was assembled with Adobe Photoshop. Each cell body is represented by a dot of about the appropriate size. Note the higher cell density in the superior and temporal quadrants. Only nondisplaced RGCs (>95% of total) are included. S, superior; I, inferior; N, nasal; T, temporal.

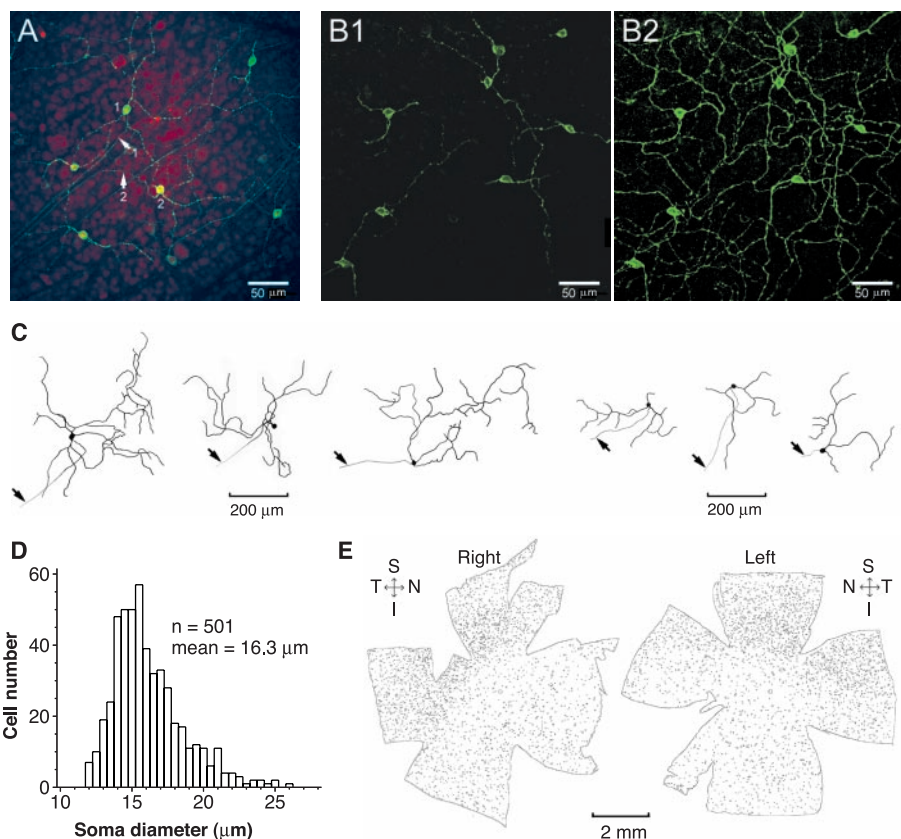
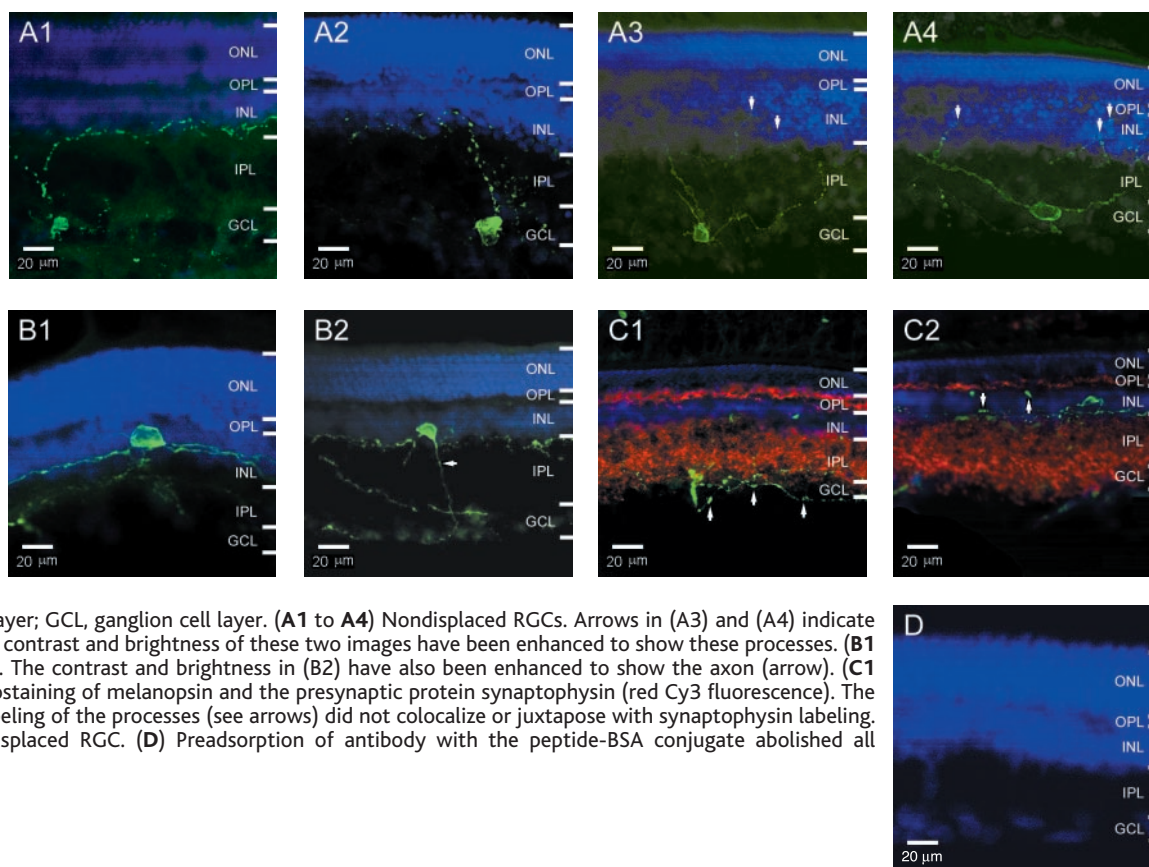


**Fig. 2.** Melanopsin-positive RGCs in cross sections of rat retina. All are single (non-stacked) confocal images from 30- $\mu$ m retinal sections, with a depth of field of only a few micrometers. Melanopsin fluorescent immunolabeling is in green and nuclear counterstaining is in blue. In all images, the brightness of the nuclear staining has been reduced to show the processes in or around the INL; as a result, the nuclear staining in the GCL is quite faint. ONL, outer nuclear layer; OPL, outer plexiform layer; INL, inner nuclear layer; IPL, inner plexiform layer; GCL, ganglion cell layer. **(A1 to A4)** Nondisplaced RGCs. Arrows in (A3) and (A4) indicate processes in the INL; the contrast and brightness of these two images have been enhanced to show these processes. **(B1 and B2)** Displaced RGCs. The contrast and brightness in (B2) have also been enhanced to show the axon (arrow). **(C1 and C2)** Double immunostaining of melanopsin and the presynaptic protein synaptophysin (red Cy3 fluorescence). The punctate melanopsin labeling of the processes (see arrows) did not colocalize or juxtapose with synaptophysin labeling. The cell in (C2) is a displaced RGC. **(D)** Preadsorption of antibody with the peptide-BSA conjugate abolished all immunostaining.



## REPORTS

pression of locomotor behavior (3), melatonin release (4), and others (5–7). Surprisingly, this non-image-forming system does not appear to originate from rods and cones. For example, rods and cones are not required for photoentrainment of circadian rhythms (8), a function mediated by the retinohypothalamic tract (9, 10) and its target, the SCN, the brain's circadian pacemaker (1). Nor are rods and cones necessary for the pupillary light reflex, mediated by the retinal projection to the pretectal region of the brainstem (2). At present, the best candidate for a photopigment is an opsin-like protein called melanopsin, which is expressed by a subset of mouse and human RGCs (11). The accompanying report (12) shows that RGCs projecting to the SCN are directly sensitive to light. Thus, melanopsin may be the photopigment responsible for this intrinsic photosensitivity, and it may also trigger other non-image-forming visual functions.

We cloned the full-length cDNA for rat melanopsin (13), on the basis of homology to

mouse melanopsin (11). The predicted amino acid sequence lacks the last 43 residues of mouse melanopsin but otherwise shows 92% identity (14). Polyclonal antibodies were generated against its NH<sub>2</sub>- and COOH-terminal sequences (15). Fluorescent immunocytochemistry (16) of flat-mounted rat retina with the antibody to melanopsin labeled a small percentage of RGCs, including cell bodies, dendrites, and axons (Fig. 1A). Somatic immunoreactivity appeared mainly at the cell surface (Fig. 1B1), suggestive of melanopsin being targeted to the plasma membrane. Every labeled retinal cell was a ganglion cell, on the basis of the presence of an axon coursing into the optic fiber layer and toward the optic disc. Axonal labeling disappeared beyond the optic disc and was not visible in the innervated targets (see below). More than 95% of labeled cell bodies were in the ganglion cell layer, the remainder being displaced to the inner nuclear layer. Dendrites from adjacent cells overlapped extensively, forming a retic-

ular network (Fig. 1B2). The stained dendrites and proximal axons had a beaded appearance, showing punctate, dense labeling. The complete dendritic fields of labeled cells, visualized from stacked confocal images (e.g., Fig. 1B2), had varied sizes and shapes (Fig. 1C). Labeled displaced RGCs (Fig. 1C, right three cells) had similar soma sizes but less extensive dendritic arborizations than nondisplaced cells (Fig. 1C, left three cells). The mean somatic diameter of labeled nondisplaced RGCs was 16  $\mu$ m (Fig. 1D), but the limited sample of dendritic-field measurements precluded any statistics. Morphologically, these neurons fit within the type III group of rat RGCs (17), especially those shown to be intrinsically photosensitive (12). The density of melanopsin-positive cells was slightly higher in the superior and temporal quadrants of the rat retina (Fig. 1E). A complete count of these cells in the two retinas of Fig. 1E gave 2320 and 2590, respectively, although some faintly labeled cells could

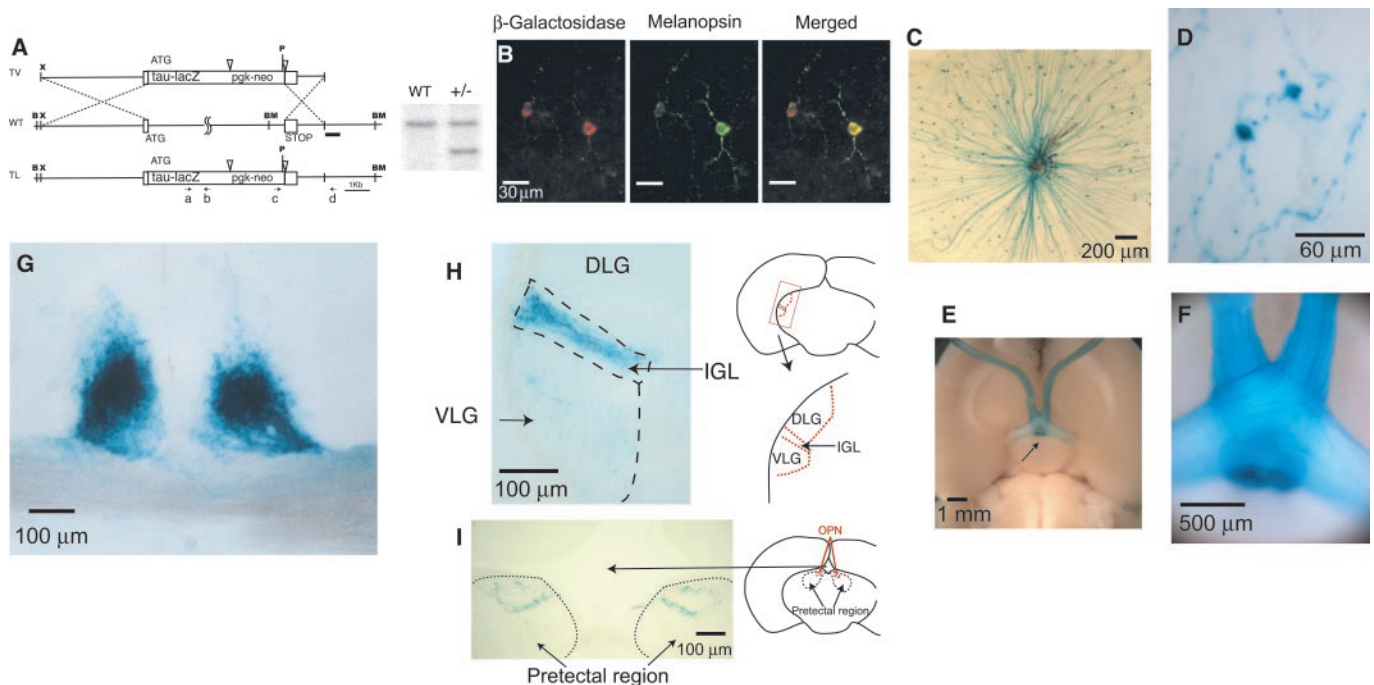


**Fig. 3.** Targeting of tau-lacZ into the mouse melanopsin gene locus. (A) (Left) Targeting strategy. In the wild-type (WT) schema, the boxes represent partial fragments of exons 1 and 9 of the melanopsin gene, with ATG indicating the start site of the melanopsin protein. The ATG in the targeting vector (TV) corresponds to the start site of the tau-lacZ fusion protein. The pgk-neo is flanked by loxP sites (open, inverted triangles) for specific cre-recombinase removal. Upon homologous recombination, the tau-lacZ fusion protein in the targeted locus (TL) retains its own start site, whereas the melanopsin start site together with the rest of the gene was eliminated. The dark bar underneath wild-type schema represents the outer probe used for screening ES cells and subsequently generated animals, by Southern (DNA) blotting. X, Xho I; B, Bgl II; BM, Bam HI; P, Pac I. The squiggles in the wild-type schema indicate a size difference of 2.6 kb between the melanopsin gene and the tau-lacZ construct. The four dotted lines indicate the homologous recombination arms used for targeting melanopsin. Primers c and d were used in PCR for screening site-specific integration of the tau-lacZ construct in electroporated ES cells. Primers a and b were used for genotyping of heterozygous animals. (Right) Genomic DNA from wild-type and

+/- mice digested with Bam HI and Pac I and hybridized with the outer probe, producing a 4.4-kb fragment in the wild-type locus and a 3.7-kb fragment in the targeted locus, as expected. (B) Colocalization of  $\beta$ -galactosidase and melanopsin immunoreactivities in a flat-mounted retina from a +/- mouse. (Left)  $\beta$ -Galactosidase labeling. (Middle) Melanopsin labeling. (Right) Merged image. (C) Flat-mount view of a +/- mouse retina stained with X-gal. Labeled axons (blue), which converge to the optic disc, are visible. The brown coloration near the optic disc is from remnants of the retinal pigment epithelium overlying the retina. (D) Magnified view of an X-gal-labeled RGC. (E) Ventral view of a +/- mouse brain stained with X-gal, showing bilateral blue staining of the SCN (arrow). (F) Magnified view of the blue-labeled axons in an optic nerve. (G) Coronal section of the +/- brain showing blue optic nerve fibers converging to, and innervating, the SCN bilaterally. (H) Coronal section of the +/- brain showing uniform blue-labeled innervation of the left IGL and scattered innervation of the VLG. The DLG shows no labeling. (I) Coronal section of the +/- brain showing innervation of the pretectal region. The blue staining corresponds approximately to the OPN, demarcated in red on the right.

## REPORTS

have been missed. Assuming 100,000 RGCs in the rat retina (18), these numbers represent about 2.5% of the total. The corresponding numbers for mouse melanopsin-immunoreactive RGCs were 680 and 780 from two eyes of one animal, or about 1% of the total [assuming 60,000 ganglion cells in a mouse retina (19)].

To locate more precisely the cell bodies and dendritic arborizations of the melanopsin-positive RGCs, we examined the rat retina in cross section (Fig. 2). Whether in the ganglion cell layer (Fig. 2A) or displaced to the inner nuclear layer (Fig. 2B), the melanopsin-expressing RGCs extended dendrites into the inner plexiform layer, where they arborized most extensively at the border with the inner nuclear layer. Some arborizations invaded and often terminated in the inner nuclear layer (arrows in Fig. 2A3 and 2A4). The displaced RGCs had dendritic arborizations that were more planar and sparse (Figs. 2B1 and 1C, right). Melanopsin-immunoreactive puncta were present throughout the dendrites, and they showed no correlation with the retinal laminae and no colocalization or juxtaposition with the presynaptic protein synaptophysin (Fig. 2C), suggesting that the puncta did not correspond to synaptic sites.

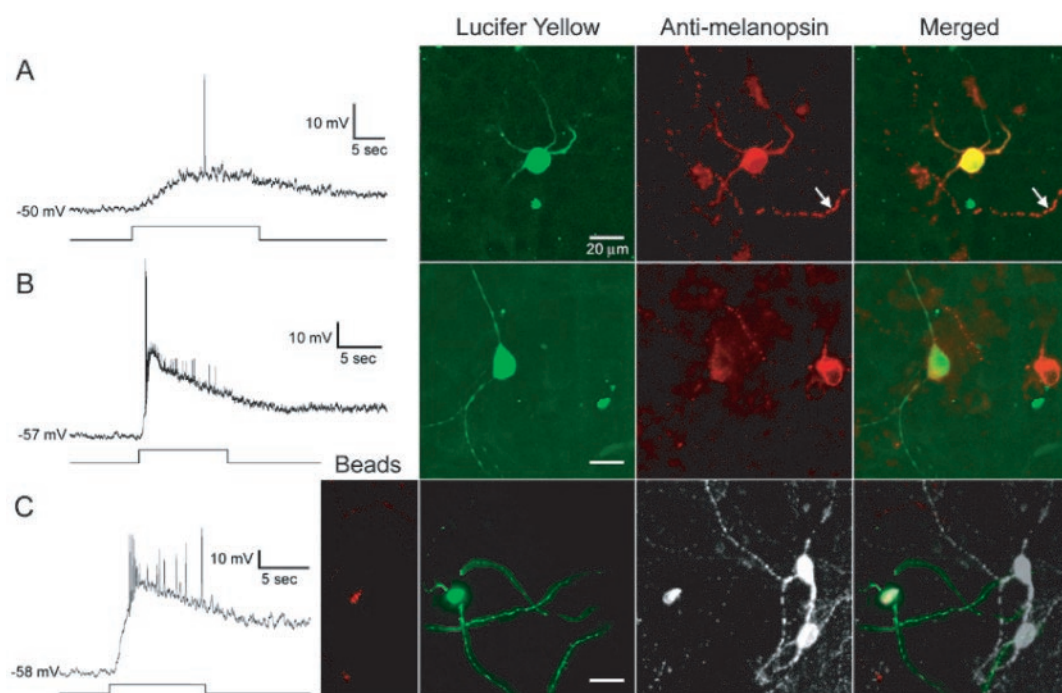
To examine the axonal projections of the

melanopsin-positive RGCs, we targeted tau-lacZ into the melanopsin gene locus in mouse (20) (Fig. 3A). Tau-lacZ codes for a protein composed of the  $\beta$ -galactosidase enzyme fused to a signal sequence from tau (an actin-associated protein), which allows the fusion protein to be preferentially transported down the axon to the presynaptic terminal (21). In retinas from heterozygous animals, which have one copy each of the melanopsin and tau-lacZ genes,  $\beta$ -galactosidase and melanopsin immunoreactivities colocalized in the ganglion cells (Fig. 3B). The morphology of the melanopsin-immunopositive cells in mouse was similar to that in rat. In X-gal labeling (22) of  $\beta$ -galactosidase activity (Fig. 3, C and D; blue color), the axons, cell bodies, and proximal dendrites were well labeled. In one heterozygous mouse retina, the total number of labeled cells was about 600, similar to the number for melanopsin-immunopositive cells in the wild-type mouse retina mentioned above. A ventral view of the brain from a heterozygous mouse showed blue-labeled axons coursing in the optic nerves and targeting the SCN bilaterally (Fig. 3, E and F). A coronal section of the brain at the SCN showed dense axonal terminations in the paired nuclei (Fig. 3G). Labeled axons continued caudally in the optic tract to the

lateral geniculate complex, terminating throughout the intergeniculate leaflet (IGL) (Fig. 3H). Stained fibers also sparsely innervated the ventral lateral geniculate (VLG) but did not invade the dorsal lateral geniculate (DLG). Labeled axons also formed a terminal field in the pretectum, in the vicinity of the olivary pretectal nucleus (OPN) (Fig. 3I). Neither melanopsin immunoreactivity nor  $\beta$ -galactosidase staining labeled neuronal somata in these or other brain regions, indicating that the axons containing melanopsin all originated from the retina.

To address whether melanopsin could be the photopigment responsible for the intrinsic light sensitivity of rat RGCs that project to the SCN (12), we injected these photosensitive RGCs intracellularly with Lucifer Yellow (LY) (23) and then stained them for melanopsin immunoreactivity. Intrinsically photosensitive ganglion cells were invariably melanopsin-positive ( $n = 18$ ; Fig. 4), whereas conventional ganglion cells lacking intrinsic light responses were melanopsin-negative ( $n = 4$ ). Thus, melanopsin is most likely the photopigment that confers the intrinsic light sensitivity to this subset of RGCs. In some photosensitive ganglion cells, individual dendrites were smoothly filled with LY but still exhibited punctate melanopsin immunoreac-

**Fig. 4.** Presence of melanopsin in intrinsically light-responsive RGCs that innervate the SCN. Sample data from three cells (A to C), all identified by retrograde transport of fluorescent rhodamine beads from the SCN before whole-cell recording from the flat-mounted retina. In each panel, the voltage trace at left shows the cell's response to a long light stimulus indicated below by the step. Broad-band tungsten light source; irradiance at retina of  $6 \times 10^{15}$  photons  $s^{-1} cm^{-2}$  at 500 nm. Bathing Ames medium contained agents to block  $Ca^{2+}$ -mediated synaptic transmission: either (A and B) 2-mM  $CoCl_2$  alone or (C) in combination with pharmacological blockers of the glutamatergic signaling between conventional photoreceptors and RGCs [100- $\mu$ M L(+)-2-amino-4-phosphonobutyric acid (APB), 20- $\mu$ M 6,7-dinitroquinoxaline-2,3-dione (DNQX), and 50- $\mu$ M DL-2-amino-5-phosphonovaleric acid (APV)] (12). Large-amplitude, fast depolarizing events are action potentials. Fluorescence images of the recorded cells are shown at right. (Left) Intracellular staining (green) with LY introduced from the whole-cell recording pipette. (Middle) Antibody to melanopsin immunofluorescence [Cy-3 fluorophore, red, in (A) and (B); Alexa Fluor 647, white, in (C)]. (Right) Superimposed fluorescence images. Far left in (C), Fluorescence of rhodamine latex beads (red), the retrograde tracer. All



micrographs are stacked, pseudocolored confocal images, except for the LY image in (C), which is a montage of optimized epifluorescence (nonconfocal, hence somewhat blurred) micrographs at different focal planes. Arrow in (A) marks the melanopsin-positive dendrite of a second ganglion cell neighboring the one recorded. In (B) and (C), other strongly melanopsin-immunopositive cells are visible near the recorded cell; these cells were not recorded from and hence showed no LY labeling.

tivity, suggesting that there may be local clusters of the opsin.

Taken together, our findings suggest that melanopsin may indeed be a photopigment, consistent with an opsin-based action spectrum demonstrated for the SCN-projecting RGCs (12). The presence of melanopsin throughout the dendritic arbors of these cells may permit spatial integration of retinal irradiance and is consistent with the extended receptive fields of these cells (12). It is unclear whether these photosensitive dendrites simultaneously serve the more conventional function of receiving synaptic inputs from rod- and cone-driven networks. There is evidence for rod and cone influences on neurons in both the SCN (24) and the OPN (2), but whether these reflect convergence at the photosensitive RGCs or convergence within the brain remains unclear. In both distribution and morphology, the melanopsin-positive RGCs described here broadly match those identified in rat and mouse retina that project to the SCN [(25–28); see also (29, 30)], although most of these other studies labeled presumably only a fraction of the cells.

Although the innervation of the SCN is the densest, the IGL, VLG, and OPN were also innervated by  $\beta$ -galactosidase-positive RGC axons in heterozygous tau-lacZ mice. Some of the fibers innervating the IGL and OPN could be collaterals of axons in the retinohypothalamic tract (31). Neurons in both IGL and OPN encode ambient light levels (32–34), a property almost certainly conferred by the photosensitive RGCs, which faithfully report retinal irradiance (12). Like the SCN, the IGL and the VLG are implicated in circadian photoentrainment (32), whereas the OPN is a key node in the circuit mediating the pupillary light reflex (33, 34), another non-image-forming visual function. Indeed, rodless and coneless mice retain a pupillary light response (2), with the spectral tuning and high thresholds expected for a response driven by the intrinsically photosensitive RGCs (12). Thus, it appears that melanopsin-containing RGCs are generally involved in non-image-forming visual functions.

References and Notes

1. D. C. Klein, R. Y. Moore, S. M. Reppert, *Suprachiasmatic Nucleus: The Mind's Clock* (Oxford Univ. Press, New York, 1991).
2. R. J. Lucas, R. H. Douglas, R. G. Foster, *Nature Neurosci.* **4**, 621 (2001).
3. N. Mrosovsky, *Chronobiol. Int.* **16**, 415 (1999).
4. D. C. Klein, J. L. Weller, *Science* **177**, 532 (1972).
5. P. Badia, B. Myers, M. Boecker, J. Culpepper, J. R. Harsh, *Physiol. Behav.* **50**, 583 (1991).
6. C. Cajochen, D.-J. Dijk, A. A. Borbely, *Sleep* **15**, 337 (1992).
7. C. Cajochen, J. Zeitzer, C. Czeisler, D.-J. Dijk, *Behav. Brain Res.* **115**, 75 (2000).
8. M. S. Freedman et al., *Science* **284**, 502 (1999).
9. R. Y. Moore, N. J. Lenn, *J. Comp. Neurol.* **146**, 1 (1972).
10. R. F. Johnson, R. Y. Moore, L. P. Morin, *Brain Res.* **460**, 297 (1998).
11. I. Provencio et al., *J. Neurosci.* **20**, 600 (2000).

12. D. M. Berson, F. A. Dunn, M. Takao, *Science* **295**, 1070 (2002).
13. Total mRNA was extracted from the retinas of an adult rat (Sprague Dawley) with MicroPoly(A) Pure Kit (Ambion, Austin, TX) and transcribed to cDNA by reverse transcriptase (SuperScriptII, Invitrogen, Carlsbad, CA) with an anchor primer, 5'-CTCTGACATAGTCTACCGCTTTTTTTTTTTTTTTT-3'. For PCR, one forward primer (5'-CACTCATCTCTTTGCGGTC-3') and two reverse primers (5'-ACAGCCCCGAGAGG-3' and 5'-GTAGAGGCTGCTGGC-3') were chosen according to the published mouse melanopsin sequence (17). Nested polymerase chain reaction (PCR) was performed in a 50- $\mu$ l volume with pfu DNA polymerase and PerfectMatch (Stratagene, La Jolla, CA) and 1/1000 of the total retina cDNA as template (35 cycles of 94°C, 3 min, 50°C, 1 min and 72°C, 30 s). One microliter of the PCR product was used as the template in a second PCR with the same thermal profile but only 25 cycles, followed by extension at 72°C for 15 min. The PCR product was ligated to the vector pGEM-T (Promega, Madison, WI) and transformed into *Escherichia coli* DH5 $\alpha$ . The resulting plasmid was sequenced (GenBank accession number AY072689). On the basis of the sequence, two new forward primers (5'-GCTCATCATCAACCTGGC-3' and 5'-GACTTCCTTATGTCGTTCAC-3') and a reverse primer (5'-CTCTGACATAGTCTACCGC-3') were used in nested 3'-RACE with the same PCR conditions as above. Several independent PCRs were performed, and the resulting DNA sequences were compared in order to reach consensus and translated into amino acids.
14. See supplementary information available on Science Online at [www.sciencemag.org/cgi/content/full/295/5557/1065/DC1](http://www.sciencemag.org/cgi/content/full/295/5557/1065/DC1).
15. The NH<sub>2</sub>-terminal peptide was KMNSPESRVPSSLTQDPSF (35), with the lysine added for cross-linking purposes. The COOH-terminal peptide was EQKSKT-PKTKRHLPLDRRM (35). They were conjugated to thyroglobulin and used to immunize rabbits (Covance, Denver, PA). The resulting antisera were purified by a peptide-bovine serum albumin (BSA)-conjugated affinity column. The specificity of the antibodies was confirmed in immunoblot experiments with melanopsin expressed in HEK 293 cells (14). In all experiments described in this paper, the NH<sub>2</sub>-terminal antiserum was used, but identical results were obtained with the COOH-terminal antiserum.
16. Whole retina or frozen 30- $\mu$ m retinal sections, after fixation in fresh 4% paraformaldehyde, were used. In the former case, the isolated whole retina was immunostained in a free-floating state, or the eyecup was immunostained before the retina was isolated for observation under the microscope. For immunolabeling, the tissue was first blocked in 5% inactivated fetal bovine serum and then incubated overnight at 4°C with the purified melanopsin antibody at 1:100 to 1:1000 dilution in phosphate-buffered saline (PBS)/0.3% Triton X-100/5% serum. After three washes of 20 min each in PBS/0.3% Triton X-100, the fluorescence-conjugated secondary antibody [Alexa Fluor 488 goat antibody to rabbit immunoglobulin G (IgG); Molecular Probes, Eugene, OR] was applied to the sample as before, except incubation was 1 to 3 hours at room temperature and the antibody was at 1:1000 dilution. In many cases, the sample was counterstained by propidium iodide (Sigma-Aldrich, St. Louis, MO) or 4',6'-diamidino-2-phenylindole (DAPI) (Molecular Probes, Eugene, OR) and mounted in VectaMount permanent mounting medium (Vector Laboratories, Burlingame, CA). For colocalization with  $\beta$ -galactosidase immunoreactivity, the primary antibody was goat antibody to  $\beta$ -galactosidase (Biotrend, Köln, Germany), and the secondary antibody was Cy3-conjugated antibody to goat IgG (Jackson Immuno Research, West Grove, PA). Otherwise, the procedure was identical.
17. V. H. Perry, *Proc. R. Soc. London* **204**, 363 (1979).
18. D. Crespo, D. D. M. O'Leary, W. M. Cowan, *Dev. Brain Res.* **19**, 129 (1985).
19. U. C. Dräger, J. F. Olsen, *J. Comp. Neurol.* **191**, 383 (1980).
20. The tau-lacZ targeting construct contained the coding sequence for a tau protein signal peptide fused to the  $\beta$ -galactosidase enzyme, as well as the neomy-

cin-resistance gene (Fig. 3A). The coding sequence was flanked by a 4.4-kb fragment 5' of the ATG start site of the mouse melanopsin gene and a 1.6-kb fragment containing 654 base pairs (bp) of exon-9 plus 946 bp 3' of exon 9, obtained from a bacterial artificial chromosome (BAC) melanopsin clone. The targeting vector was linearized by Xho I and electroporated into 129.1 mouse strain embryonic stem (ES) cells, and the latter was subsequently selected by G418 (300  $\mu$ g/ml) with standard procedures. Two hundred resulting ES cell clones were screened by PCR and DNA blotting, with one found to have incorporated the targeting vector appropriately. It was injected into C57/Bl6 blastocysts and introduced into pseudopregnant females. Chimeric animals were mated to C57/Bl6 mice to produce agouti heterozygous animals.

21. P. Mombaerts et al., *Cell* **87**, 675 (1996).
22. For X-gal labeling of whole brain, brain sections, or retina, an animal anesthetized by intraperitoneal injection of Avertin (0.2 ml/g) was circulationally perfused with 25 ml of cold 4% paraformaldehyde in PBS for 10 min, and the brain or eyes were isolated and stained with X-gal for  $\beta$ -galactosidase activity, according to Mombaerts et al. (21). The fixed brain was washed twice (5 min and 30 min, respectively) in buffer A (100 mM phosphate buffer at pH 7.4, 2 mM MgCl<sub>2</sub>, and 5 mM EGTA) and twice in buffer B [100 mM phosphate buffer at pH 7.4, 2 mM MgCl<sub>2</sub>, 0.01% Na-desoxycholate, and 0.02% (Octylphenoxy) polyethoxyethanol (IGEPAL)]. It was then incubated in the staining solution [buffer B plus 5 mM K-ferricyanide, 5 mM K-ferrocyanide, and X-gal (1 mg/ml)] for 6 to 30 hours at room temperature in darkness. The stained brain was sectioned at 100- $\mu$ m thickness with a vibratome after embedding in 4% low-melting agarose. For labeling of the retina, the anterior half of the eye was removed, and the posterior eyecup was stained with X-gal for 24 to 30 hours at 37°C in darkness. Afterwards, the retina was isolated and mounted in glycerol.
23. The retrograde labeling of RGCs by dye injection into the SCN and subsequent recording procedures are as described elsewhere (12). Adult rats were anesthetized with ketamine (60 mg/kg) and medetomidine (0.4 mg/kg, intraperitoneally). Rhodamine-labeled fluorescent latex microspheres (Lumafuor; 0.1 to 0.3  $\mu$ l) were deposited unilaterally into the hypothalamus through glass pipettes tilted 10° from vertical. In 2 to 20 days after injection, rats were anesthetized (Nembutal, 120 mg/kg, ip), eyes were removed and hemisected, and eyecups were rinsed in enzyme solution [collagenase/dispase (2 mg/ml) and deoxyribonuclease (DNase) (0.1 mg/ml) in Ames medium; 1 min] to remove vitreous. Retinas were isolated, mounted in a chamber (Warner RC-26G/PL), and superfused at room temperature with bicarbonate-buffered Ames medium. Microsphere-labeled ganglion cells were viewed on the stage of an upright microscope and identified by epifluorescence, and their somata were exposed by microdissection. Whole-cell current clamp recordings were made with patch pipettes (3 to 7 megaohms) containing 125 mM K-gluconate, 5 mM NaCl, 4 mM KCl, 10 mM EGTA, 10 mM Hepes, 4 mM adenosine triphosphate-Mg, 7 mM phosphocreatine, 0.3 mM guanosine triphosphate-tris, LY (0.1% w/v), and biocytin (0.5% w/v). Resting potentials were not corrected for liquid junction potentials. Light stimuli were introduced from below with the microscope's 100-W tungsten-halogen lamp and transillumination optics. Detachment from pigment epithelium and exposure to bright light during dissection ( $\sim 1 \times 10^{17}$  photons s<sup>-1</sup> cm<sup>-2</sup> measured at 500 nm) and epifluorescence examination ( $\sim 3 \times 10^{17}$  photons s<sup>-1</sup> cm<sup>-2</sup> at 560 nm) should have strongly bleached rod and cone photopigments. Furthermore, we added to the superfusing Ames medium 2 mM CoCl<sub>2</sub>, which blocks synaptic transmitter release from rat rods and cones (36) and abolishes the robust light responses of conventional ganglion cells in rat eyecup preparations (37).
24. N. C. Aggelopoulos, H. Meissl, *J. Physiol.* **523**, 211 (2000).
25. R. Y. Moore, J. C. Speh, J. P. Card, *J. Comp. Neurol.* **352**, 351 (1995).

26. I. Provencio, H. M. Cooper, R. G. Foster, *J. Comp. Neurol.* **395**, 417 (1998).
27. J. Hannibal et al., *J. Neurosci.* **17**, 2637 (1997).
28. J. Hannibal, M. Moller, O. P. Ottersen, J. Fahrenkrug, *J. Comp. Neurol.* **418**, 147 (2000).
29. J. J. Gooley, J. Lu, T. C. Chou, T. E. Scammell, C. B. Saper, *Nature Neurosci.* **4**, 1165 (2001).
30. J. Hannibal, P. Hindersson, S. M. Knudsen, B. Georg, J. Fahrenkrug, *J. Neurosci.* **22**, 1 (RC191) (2002).
31. G. E. Pickard, *Neurosci. Lett.* **55**, 211 (1985).
32. M. E. Harrington, *Neurosci. Biobehav. Rev.* **21**, 705 (1997).
33. L. J. Trejo, C. M. Cicerone, *Brain Res.* **300**, 49 (1984).
34. R. J. Clarke, H. Ikeda, *Exp. Brain Res.* **57**, 224 (1985).
35. Single-letter abbreviations for the amino acid residues are as follows: A, Ala; C, Cys; D, Asp; E, Glu; F, Phe; G, Gly; H, His; I, Ile; K, Lys; L, Leu; M, Met; N, Asn; P, Pro; Q, Gln; R, Arg; S, Ser; T, Thr; V, Val; W, Trp; and Y, Tyr.
36. D. G. Green, N. V. Kapousta-Bruneau, *Vis. Neurosci.* **16**, 727 (1999).
37. F. A. Dunn, personal communication.
38. We thank R. R. Reed, and S. S. Wang and H. Zhao in his laboratory, for the tau-lacZ construct and invaluable advice. We also thank I. Provencio for providing the melanopsin BAC clone, J. Nathans and H. Sun for discussions, K. Takamiya, Y. Zhang, S. A. Ralls, M. Dehoff, B. E. Lonze, and especially M.

Cowan and the Johns Hopkins Transgenic Facility for technical help/advice in the generation of the tau-lacZ knock-in mice as well as providing the ES cells. We are grateful to R. Richardson and S. Carlson for technical assistance with the experiments on colocalization of melanopsin and intrinsic photic sensitivity. Finally, we thank R. Masland and members of the Yau laboratory, especially J. Bradley, W.-H. Xiong, and H. Zhong, for help/critique on the experiments. This work was supported by grants from the U.S. National Eye Institute to D.M.B. and K.-W.Y.

7 January 2002; accepted 11 January 2002

## Phototransduction by Retinal Ganglion Cells That Set the Circadian Clock

David M. Berson,\* Felice A. Dunn,† Motoharu Takao†

Light synchronizes mammalian circadian rhythms with environmental time by modulating retinal input to the circadian pacemaker—the suprachiasmatic nucleus (SCN) of the hypothalamus. Such photic entrainment requires neither rods nor cones, the only known retinal photoreceptors. Here, we show that retinal ganglion cells innervating the SCN are intrinsically photosensitive. Unlike other ganglion cells, they depolarized in response to light even when all synaptic input from rods and cones was blocked. The sensitivity, spectral tuning, and slow kinetics of this light response matched those of the photic entrainment mechanism, suggesting that these ganglion cells may be the primary photoreceptors for this system.

The SCN is the circadian pacemaker of the mammalian brain, driving daily cycles in activity, hormonal levels, and other physiological variables. Light can phase-shift the endogenous oscillator in the SCN, synchronizing it with the environmental day-night cycle. This process, the photic entrainment of circadian rhythms, originates in the eye and involves a direct axonal pathway from a small fraction of retinal ganglion cells to the SCN (1–3). A striking feature of this neural circuit is its apparent independence from conventional retinal phototransduction. In functionally blind transgenic mice lacking virtually all known photoreceptors (rods and cones), photic entrainment persists with undiminished sensitivity (4). Candidate photoreceptors for this system are nonrod, noncone retinal neurons, including some ganglion cells, that contain novel opsins or cryptochromes (5–8).

To determine whether retinal ganglion cells innervating the SCN are capable of phototransduction, we labeled them in the rat retina by retrograde transport of fluorescent microspheres injected into the hypothalamus

(9). In isolated retinas, whole-cell recordings were made of the responses of labeled ganglion cells to light (10) (Fig. 1, A to E). In most of these cells ( $n = 150$ ), light evoked large depolarizations with superimposed fast action potentials (Fig. 1, E to G) (11). The light response persisted during bath application of 2 mM cobalt chloride (Fig. 1F;  $n = 42$ ), which blocks calcium-mediated synaptic release from rods, cones, and other retinal neurons (12). In contrast, other ganglion cells prepared and recorded under identical conditions but not selectively labeled from the SCN (control cells) lacked detectable response to light even without synaptic blockade (47/50 cells; Fig. 1, I and J) (13). This is presumably because rod and cone photopigments were extensively bleached (10). A few control cells (3/50) exhibited weak, evanescent responses to light, but these were abolished by bath-applied cobalt ( $n = 2$ ).

To ensure blockade of conventional synaptic influences from rods and cones, we supplemented cobalt with a mixture of drugs that independently disrupted both the glutamatergic synapses crucial to vertical signal transfer through the retina and the ionotropic receptors responsible for most inhibitory influences on ganglion cells (14). Robust light responses persisted in SCN-projecting ganglion cells under these conditions (Fig. 1G;  $n = 7$ ). Furthermore, the somata of these

ganglion cells exhibited photosensitivity even when completely detached from the retina by microdissection (Fig. 1H;  $n = 3$ ). These light responses were not an artifact of photic excitation of either of the intracellular fluorophores we used, as the action spectrum of the light response (Fig. 2C) differed from the absorption spectra of both the retrograde tracer and Lucifer Yellow (LY) used for intracellular staining. Also, light-evoked increases in spike frequency were detectable in extracellular recordings, before patch rupture and LY dye filling ( $n = 5$ ). Whole-cell recordings revealed normal light responses when LY was omitted from the internal solution ( $n = 8$ ). In contrast, control cells lacked cobalt-resistant light responses even when labeled with both fluorescent beads and LY ( $n = 12$ ; Fig. 1I). These data indicate that retinal ganglion cells innervating the SCN are intrinsically photosensitive.

To determine if these cells could serve as the primary photoreceptors for circadian entrainment, we assessed congruence between their photic properties and those of the entrainment mechanism. The responses of a single cell to narrow-band stimuli of various intensities showed that at each wavelength, peak depolarization increased with stimulus energy (Fig. 2, A and B). Intensity-response curves exhibited a consistent slope when plotted in semilogarithmic coordinates (Fig. 2B), as expected for responses mediated by a single photopigment (principle of univariance). The horizontal displacements of the curves from one another reflect the spectral dependence of the pigment's quantum efficiency and yield the spectral sensitivity function shown in Fig. 2C (red curve). Other cells exhibited similar action spectra (Fig. 2C, green curve) (15). These action spectra closely matched that predicted for a retinal,  $\gamma$ -based pigment with peak sensitivity at 484 nm (Fig. 2C, black). They also resemble action spectra derived behaviorally for circadian entrainment in rodents (16, 17), as expected if these ganglion cells function as primary circadian photoreceptors (18). Judging from available spectral evidence, the photopigment in these ganglion cells is more likely to be a retinaldehyde-based opsin such as melanopsin (5, 19, 20) than a flavin-based cryptochrome (21).

Department of Neuroscience, Brown University, Providence, RI, 02912 USA.

\*To whom correspondence should be addressed. E-mail: David\_Berson@brown.edu

†These authors contributed equally to this work.